Defense Technical Information Center Compilation Part Notice

ADP023844

TITLE: Combustion Chamber Fluid Dynamics and Hypergolic Gel Propellant Chemistry Simulations for Selectable Thrust Rocket Engines

DISTRIBUTION: Approved for public release, distribution unlimited

This paper is part of the following report:

TITLE: Proceedings of the HPCMP Users Group Conference 2004. DoD High Performance Computing Modernization Program [HPCMP] held in Williamsburg, Virginia on 7-11 June 2004

To order the complete compilation report, use: ADA492363

The component part is provided here to allow users access to individually authored sections of proceedings, annals, symposia, etc. However, the component should be considered within the context of the overall compilation report and not as a stand-alone technical report.

The following component part numbers comprise the compilation report:
ADP023820 thru ADP023869

Combustion Chamber Fluid Dynamics and Hypergolic Gel Propellant Chemistry Simulations for Selectable Thrust Rocket Engines

Michael J. Nusca and Michael J. McQuaid

US Army Research Laboratory (ARL), Weapons and Materials Research Directorate, Aberdeen Proving Ground, MD

{nusca, mcquaid}@arl.army.mil

Abstract

The Army is developing gelled bipropellants and tactical missile propulsion systems that utilize these propellants for future combat systems. The use of hypergolic gel propellants introduces new capabilities for selectable thrust missiles while at the same time introducing new challenges in combustion control, one of which is the mixing of oxidizer and fuel to obtain maximum performance without increasing the size of the engine. One of the Army's leading propulsion candidate's, the impinging stream vortex engine (ISVE), has generated excellent performance test data. Since the ISVE is a new concept, analytical models are just beginning to emerge. However, in order to fully exploit the performance advantages of the ISVE it is desirable to understand the underlying flow physics of the engine. This paper describes a high performance computing methodology that is producing simulations of the ISVE using computational fluid dynamics to model the chemically reacting flow within the engine and computational chemistry to characterize the hypergolic bipropellants.

1. Introduction

A common, modular, small, low cost precision guidance weapon is required by the Army's Research Development and Engineering Command (RDECOM) in order to support the Army's Future Combat Systems (FCS) and to meet the needs of the Objective Force. This weapon (missile system) must be capable of engaging soft and lightly armored point targets with minimal collateral damage. In contrast, current lethality options being developed for the FCS are focused on defeating heavily armored targets with less emphasis on soft and lightly armored point targets. Therefore, a complementary, low cost, small diameter weapon system to engage soft targets

with surgical strike precision is required for the FCS. The 2.75-inch guided rocket currently being demonstrated in the Low Cost Precision Kill (LCPK) Advanced Technology Demonstrator (ATD) and the Advanced Precision Kill Weapon System (APKWS) provides this capability but uses a large missile airframe. In contrast, the FCS requires a significantly shorter missile as current airframes are too long for integration into the FCS platforms.

In order to directly address these needs, the Aviation and Missile Research Development and Engineering Center (AMRDEC) and the Army Research Laboratory (ARL), both within the RDECOM are engaged in a high-priority Strategic Technology Objective (STO). The Advanced Miniature Multi-Role Precision Guided Missile Technology (AMMPGM) STO addresses key technologies that enable the 2.75-inch guided rocket to be significantly shortened while retaining performance. Concurrently, the Army has identified the need for missile systems with thrust modulation over wider ranges (i.e., higher turn down ratios) than those achievable with current technology. Research in this area has yielded gelled propellant engines that have been flown as propulsion systems and throttled to actively change the trajectory of the missile—thus the "selectable thrust" characteristic. Gelled propellants can produce a theoretical specific impulse, ISP (thrust produced by the engine normalized by the weight of the engine's through-flow) of 275–280 seconds—an impressive performance metric. The average solid propellant rocket delivers an ISP of 250 seconds or less and cannot be throttled. One such gelled oxidizer/fuel combination consists of inhibited red fuming nitric acid, IRFNA, and monomethyl hydrazine, MMH. Along with the advantages of "selectable thrust", the use of gel propellants for missile propulsion introduces new challenges in flow and combustion control. Due to increases in chamber pressure

180

and reduction in injector pressure, the gels pose challenges for optimal fuel/oxidizer mixing time, which must be as short as possible in order to obtain maximum performance from the combustor. For conventional missile engines, mixing difficulties are typically overcome by increasing the chamber volume available for combustion with a corresponding increase in engine weight—a consequence not acceptable to the AMMPGM STO or the FCS program.

1.1. The Impinging Stream Vortex Engine.

The impinging stream vortex engine, ISVE[1,2] that is being developed at the AMRDEC, is currently the leading propulsion unit being considered in the AMMPGM STO. The ISVE, shown schematically in Figure 1, is radically different from the conventional impinging stream engine (ISE). In the ISVE propellants are injected tangentially to the chamber wall, impinge, and then swirl via the vortex flow that is generated by this tangential injection component. The initial mixing occurs during stream impingement and the final mixing occurs in the highly turbulent vortex region between the injector orifices and the chamber walls. There has been some evidence from post-test examination of the engine hardware that the heavier solid particles separate from the gas particles and move toward the chamber walls. It has been postulated that centrifugal movement of the solid particles increases the path length and thus increases the fluid transit time in the combustion zone. Since the efficiency of fuel/oxidizer mixing is related to this transit time, the real advantage of the ISVE is that the engine's L^* (defined as the combustor volume divided by the area of the sonic throat, that is directly proportional to the fluid transit time) can be made much smaller thereby decreasing the size and weight of the engine. An additional attribute of the vortex injection concept is that the propellants provide transpiration cooling, protecting the radial chamber wall from the combustion flame. Testing of the ISVE has yielded delivered specific impulse efficiencies of 250–255 sec for an L^* of 5 inches using IRFNA as oxidizer and 50 percent carbon-loaded MMH as the fuel. For the conventional ISE the delivered ISP is 260–265 sec (i.e., closer to theoretical 275–280 sec) but at the cost of increasing the L^* to 10 or 20 inches (i.e., larger engine)[1].

Since the ISVE is a relatively new concept, the databases and analytical models relating performance to the engine design parameters (such as size) are just beginning to be formulated. In order to fully exploit the performance advantages that have been realized for the ISVE and to optimize the engine at other scales, it is desirable to understand the underlying flow physics of the engine. In particular, the small time delay between fuel/oxidizer injection, rapid pressurization of the

combustion chamber, and chamber wall cooling are important performance features. To address these issues, a cooperative effort was initiated between the AMRDEC and the Army Research Laboratory[3].

1.2. Gelled Hypergolic Propellants.

An integral aspect of the ISVE engine design is the performance characteristics of the fuel and oxidizer gels. The main ingredient in the fuel gel—i.e., the one that makes it hypergolic—is monomethylhydrazine (MMH). The oxidizer is primarily inhibited red fuming nitric acid (IRFNA)—its main components being nitric acid (HNO_3) and nitrogen dioxide (NO_2). The superior performance of this fuel-oxidizer combination is attributable to several factors. One is its extremely short "ignition delay"—i.e., the time that elapses between the onset of the combination's mixing in combustion chamber and the establishment of gas-phase combustion. The rapid combustion of propellant that accumulates in a combustion chamber prior to ignition produces a pressure excursion that scales with the ignition delay, and the combustion chamber must be sized to accordingly. MMH has the shortest ignition delay (with IRFNA) of any fuel yet tested. Therefore, its use facilitates the design of the smallest rocket motors. Another beneficial attribute of the MMH-IRFNA combination is its high density specific impulse ($\rho*Isp$).

Despite the long service of MMH-IRFNA combinations in rocket propulsion applications, the chemistry underlying their ignition and combustion remains largely speculative. This, in turn, raises questions about whether the CFD model's ability to reproduce ISVE test results is part happenstance. Also, the MMH fuel gel currently being utilized could be improved. For one, the gellants employed for MMH and IRFNA are different, which may limit the efficiency with which they mix. And gellant masses being parasitic, fuel formulations with reduced gellant loadings are being sought. Finally, MMH is acutely toxic and a suspected carcinogen. Therefore, its use requires the implementation of costly and burdensome handling procedures; an alternative is desirable. Thus, beyond being needed as input for the CFD model, the characterization of fuel and oxidizer gel properties could lead to enhanced formulations.

1.3. The Coupled HPC Effort.

High performance computing (HPC) is required to produce timely simulations of combustion chamber gas dynamics and engine performance parameters (using computational fluid dynamics—CFD) as well as hypergolic gel propellant chemistry characterizations (using computational chemistry and material science—

CCM) for the ISVE. Both the CFD and the CCM parts of this HPC effort were necessarily coupled efforts since the CFD simulations cannot definitively compute the chemically reacting flowfield within the ISVE (and thus performance) without input from the CCM simulations that detail the chemical, kinetic, and thermodynamic properties of existing and newly discovered gel propellants. In the remainder of this paper we report overviews of both the CFD and the CCM technical approaches, the specific results achieved to date, and a detailing of the HPC hours used in these efforts.

2. Computational Fluid Dynamics Code

The high-temperature, non-ideal, chemically reacting gas flow field within the ISVE is numerically simulated using CFD. The ARL-NSRG3 code was written by the first author[4,5] to solve the 3D, unsteady, real-gas Navier-Stokes equations. Computational submodels that represent finite-rate (nonequilibrium) chemical kinetics, multi-species diffusion and thermodynamic properties (specific heats), non-Newtonian viscosity, turbulence, and droplet vaporization/decomposition augment these equations. The Navier-Stokes equations for 3D (x,y,z coordinates) reacting (N species), Newtonian, and unsteady (time, t) flow are given below in nondimensional, conservative form. The dependent variables are density (ρ), velocity (V and components u,v,w), energy (e), and species mass fraction (c_i). Pressure and temperature are p and T while L is a characteristic length scale for the flow field.

$$\frac{\partial U}{\partial t} + \frac{\partial F}{\partial x} + \frac{\partial G}{\partial y} + \frac{\partial H}{\partial z} + J = 0$$

$$U = \left\{\rho, \rho u, \rho v, \rho w, \rho e, \rho c_1, ..., \rho c_N\right\} \quad J = \left\{0, 0, 0, 0, 0, -\omega_1, ..., \omega_N\right\} \quad (1)$$

The F, G, and H arrays contain flux terms (convective and diffusive), heat transfer terms and stress terms (normal and shear). The J array contains the chemical production terms for each species. For a more complete description of the governing equations, constitutive and state relations and the numerical solution scheme, the reader is referred to papers by Nusca et al.[3–5] Since the viscosity enters these equations through the Reynolds number and the stress terms, and since non-Newtonian effects are inherent in gelled propellants, a discussion of this parameter can be found in References 3, 6, and 7. The turbulent component of viscosity is computed by solving a separate differential equation for μ_t that has been formulated by Spalart and Allmaras[8].

A chemical source term appears in Eq. 1 (J term) or each species, i, denoted, ω_i. This term is determined using a chemical kinetics mechanism that is prescribed for the

problem under consideration. Chemical reactions can be expressed in a general reaction rate equation with stoichiometric coefficients for species in these reactions. The chemical source terms in the J array (i.e., ω) are computed using a general reaction rate equation,

$$\frac{dC}{dt} = \frac{\omega_i}{M_i} = \left(v_i^{''} - v_i^{'}\right)\left(k_f \prod_i^N C_i^{v_i^{'}} - k_b \prod_i^N C_i^{v_i^{''}}\right) \quad (2)$$

where the C_i above represents concentration which is raised to powers of either the reactant coefficient (v-prime) or product coefficient (v-double-prime). The forward reaction rate is,

$$k_f = C \, T^n \exp(-E / kT) \quad (3)$$

where the rate data: C, E, and n are defined in a kinetics mechanism. The fuel consists of MMH (CH_3NHNH_2) and the oxidizer consists of IRFNA ($H_{.8894}N_{.9635}O_{2.6989}$) or more simply nitric acid, HNO_3. Thus there are two reactants. An equilibrium analysis indicates that there are 14 major products of combustion: O_2, N_2, CO_2, CO, H_2, H, H_2O, H_2O_2, HO_2, HNO, NO, NO_2, O, and OH. It can be assumed that the fuel and oxidizer react in a hypergolic fashion (i.e., very fast reaction rate) when present in the specified proportions (e.g., oxidizer/fuel ratio). The stoichiometric coefficients of the product species for an assumed one-step reaction are determined using a typical execution of the NASA-Lewis equilibrium thermodynamics code[9] using an oxidizer/fuel ratio of 2.6. Using this one-step reaction in the CFD code yields results that are quite sensitive to the choice of rate constants (C, n, and E in Eq. 3). After sensitivity analyses were conducted (see Reference 3), C was chosen as 100 with n and E chosen as zero (i.e., the reaction rate is constant). A multi-step reaction mechanism has been formulated by Dr. William Anderson of the ARL for MMH and HNO_3. This mechanism consists of 72 species and 489 reactions with rate data (C, n, E) available for each reaction and is scheduled to be published.

The propellants are injected into the ISVE as gels that atomize into liquid droplets within the combustion chamber. A two-phase flow is assumed in which the dispersed phase is in the form of discrete single-component spherical liquid droplets with a density that is much larger than the density of the ambient gas in the chamber. The momentum exchange between the droplets and the gas is assumed to be only a function of the drag force. The thermal energy exchange between the gas and liquid phases is assumed to occur only through convection with the internal droplet vertical flow neglected. These assumptions along with some others embody the classical rapid mixing model (or D^2 model). See References 3 and 10 for details. Lastly, it is assumed that the droplets are of uniform initial (or injection) diameter, D = 50 μm, and temperature (300K). The density of the IRFNA droplet is

1590 kg/m^3, the density of the MMH droplet is 880 kg/m^3, and the latent heat of evaporation is 428 kJ/kg for both the IRFNA and the MMH droplets.

2.1. Application to the ISVE.

Figure 2 shows the computational grid (203 cells along the chamber axis and 200 cells across the chamber diameter) constructed in each of 180 azimuthal planes, for a total of about 7 million grid cells within the three-dimensional geometry. Note that not all grid cells in this single azimuthal plane are displayed in the figure; rather every other cell has been plotted for clarity. The combined combustion chamber and nozzle is 7.5 cm long and 2.8 cm in diameter (the figure has not been plotted to scale). In the ISVE, fuel and oxidizer are injected into the engine through pairs of injector orifices located around the chamber's radial wall (Figure 1). For each pair of orifices, one orifice carries fuel and the other carries oxidizer. The orifices are also slightly slanted toward each other (fuel injector at 22 degs. and the oxidizer injector at 15 degs. from the chamber wall) so that the fuel and oxidizer streams within each pair immediately impinge. In addition, the orifices are slanted slightly in the azimuthal direction (fuel injector at 45 degs. and the oxidizer injector at 20 degs. from the chamber wall) so that the impinging fuel/oxidizer streams begin with an azimuthal velocity component, i.e., swirl. The location of these injector pairs is indicated on Figure 2 by black arrows (the azimuthal plane displayed cuts through two pairs of injector orifices located 180-degrees apart). The orifices are not explicitly represented in the simulation, rather fuel/oxidizer are injected into the grid cell adjacent to the chamber wall at these locations.

The particular engine design displayed in Figures 1 and 2 is designated Engine No. 1 that belongs to a family of ISVE designs being tested at the AMRDEC. A different engine design, designated Engine No. 5, has a chamber length/diameter ratio twice that of Engine No.1, an overall length/diameter of about 3.5 (2.5 for No.1) and twice as many injector pairs. In addition, Engine No. 5 has an oxidizer flow rate and a fuel flow rate which are 40% and 10% higher, respectively, as compared to Engine No. 1. In order to test the ARL-NSRG3 CFD code, results from both of these designs will be presented in this paper.

In practice, oxidizer alone is injected into the chamber of the ISVE until the approximate time in which fully developed (choked) flow is established in the engine. At this time, fuel is injected. During injection, the fuel and oxidizer lines are pressurized to about 2600 psia. Consequently, the prescribed initial injection rates are reduced over time by the diminishing pressure differential between these lines and the chamber. At the time of

injection for Engine No. 1, the oxidizer flows into the chamber at about 130 m/s and the fuel at about 190 m/s, while at the time of steady engine operation (i.e., oxidizer flow rate of .532 lb$_m$/s and fuel flow rate of .208 lb$_m$/s) these velocities have decreased to about 50 m/s and 70 m/s, respectively. The ARL-NSRG3 code was setup for just such a scenario.

Figure 3 shows the computed pressure results (red, green and blue curves) as compared to measurements (black curves). The pressure tap is located at the chamber's closed end, called the "head-end" (see Figure 1). In the case of the experiment for Engine No. 1, the oxidizer was injected continuously from 0.35s and the chamber pressure reached about 900 psia before fuel was injected (starting from .39s) and combustion started; the final pressure level was about 1850 psia. A similar engine start scenario was used for Engine No. 5. The computations utilizing the one-step reaction (green curve) and the multi-step reaction (red curve) mechanisms are shown along with a simulation that did not permit chemical reaction (blue curve). Since chemical reactions are not occurring during the oxidizer injection phase, all of the computational results show a similar initial pressurization (i.e., 900–1000 psia) when compared to the experimental measurements. It is during this time that the engine flow is established in the chamber and through the nozzle.

Immediately after the time of fuel injection, the pressure measurements for both engine designs show a distinct pressure transient (i.e., pressure peak) which results from the hypergolic combustion of fuel and oxidizer. A steady engine pressure (i.e., 1800–2200 psia) with some degree of acoustic instability follows this transient. Overall, the computations that use the multi-step reaction mechanism show the best agreement with both the transient and steady-state pressures; the simulation with one-step chemistry either under or over predict the hypergolic transient. Recall that the one-step reaction was run with a selected reaction rate chosen to achieve the best agreement with the steady pressure data. The multi-step reaction chemistry requires no such rate calibration. Both the measurements and the computations show that Engine No. 5 yields the higher steady chamber pressures due mainly to the increased number of injectors and propellant flow rates.

From the results shown in Figure 3, it can be concluded: 1) the gas dynamics of the engine are represented well by the model, 2) the reaction rate for the one-step reaction was calibrated for Engine No. 1 and thus this mechanism does not perform as well for Engine No. 5, 3) the multi-step reaction mechanism does not require rate calibration and performs equally well for both engine designs, 4) the multi-step reaction mechanism captures both the transient pressure peak due to hypergolic ignition and the steady pressure level in the

engines, and 5) the model does not presently contain the appropriate physics to represent the acoustic instability of the engine.

Figures 4 and 5 show pressure contours in Engine No. 1 and No. 5 for times at which the flowfield in the combustion chamber has reached a steady-state (recall Figure 3). The multi-step reaction mechanism was utilized. Injection of reactants and the stagnation of flow in the chamber have generated high-pressure regions around the injectors and near the top of the chamber (i.e., the closed end of the chamber shown at the left in the figures). The slant of the flowfield toward the top of the chamber is caused by the strong oxidizer injection in that direction, opposed by a weaker fuel injection stream directed toward the engine nozzle. For Engine No. 5, higher pressures are realized along the centerline of the chamber at the closed end (i.e., away from the location of the experimental pressure tap); recall that in Figure 3 the computed pressure peak for Engine No. 5 is shown as smaller than that for Engine No. 1.

Figures 6 and 7 show contours of OH mass fraction in Engine No. 1 and No. 5 for times at which the flowfield in the combustion chamber has reached a steady-state (same times as shown in Figures 4 and 5). The multi-step reaction mechanism was utilized. The species OH is one of the most prominent reaction products and indicates the region of significant heat release in the flowfield. One notable difference in these flowfields is that most of the reaction occurs both at the injection sites and the top of the chamber for Engine No. 1 while principally at the injectors for Engine No. 5. This may be caused by the closer proximity of the injectors to the top chamber wall for Engine No. 1, which allows less time for complete combustion. Overall the flowfields within the two engines are quite similar with subtle differences indicated in both the measurements and the computations of pressure (recall Figure 3).

Figures 8 and 9 show the computed OH mass fraction contours at the same times for Figures 6 and 7 but with the one-step reaction mechanism being utilized in the simulation. Note that the contour levels have been significantly reduced, relative to Figures 6 and 7, to account for the smaller amounts of OH produced using this mechanism. The one-step reaction mechanism results in major product and heat release downstream of the injectors while the multi-step reaction mechanism shows continual production of OH near the top of the chamber. A close examination of these simulations reveals that the one-step reaction produces large quantities of OH (along with other species) immediately at the injection sites and that these gases are convected toward the nozzle over time. Using these results it can be concluded that the multi-step reaction mechanism is more appropriate for simulations of the ISVE. From a computational standpoint, the multi-step mechanism requires approximately 30% more computer time per simulation.

3. Computational Chemistry Code and Results

During the initial stages of this effort, the computational chemistry effort has had two focuses. The first was to complete a study of a correlation observed between an alkyl multiamine's ignition delay and the orientation of its lone pair sites with respect to C-N or C-C bonds. Conducted in the hope of establishing a criterion for predicting the ignition delays of such compounds, the properties of two notional compounds proposed to address other shortcomings of these potential alternatives to MMH were also characterized. The second was to map the energetics of H-atom abstraction from hydrazine, MMH and unsymmetrical dimethylhydrazine (UDMH) by NO_2. These reactions hypothesized to be rate limiting steps in the ignition process, the study was undertaken to examine the hypothesis and to evaluate the reaction rates that have been specified for it in the CFD code's finite rate chemical kinetics mechanism.

Both studies rely primarily on computational quantum mechanics (QM) methods. The Gaussian 03 suite of quantum chemistry codes[11] was employed for all such calculations. For the study of alkyl multiamines, the G03 implementation of PBEPBE/6-311++G(d,p)[12-17] was employed to identify equilibrium molecular structures. Conformer searches for a given molecule were conducted by starting geometry optimizations from all of the structures that can be hypothesized for it based on presumed dihedral angle preferences. The Gaussian-defined "tight" convergence criteria (i.e., Maximum Force ≤0.000015 Hartree/Bohr, Root Mean Square (RMS) Force ≤0.000010 Hartree/Bohr, Maximum Displacement ≤0.000060 Bohr, and RMS Displacement ≤0.000040 Bohr) were employed to indicate that a local minimum had been found, and normal mode frequencies were then calculated to confirm the equilibrium structure. The normal mode calculation also provided a zero-point correction. Zero-point corrected energies (ZPE) were employed as the basis for comparing energies of a molecule's conformers (ΔE_i's) and to estimate conformer statistical weights (W_i) in a vapor sample at 298 K.

In addition to identifying and characterizing alkyl multiamine structures, properties needed to compute a fuel-IRFNA combination's $\rho*Isp$ were calculated. These properties include: (1) gas-phase enthalpies of formation, (2) enthalpies of vaporization, and (3) densities. Gas-phase enthalpies of formation at 298 K [$\Delta H_f(298)$] were derived from the enthalpies of reaction [$\Delta H_r(298)$] calculated for "isodesmic" reactions at 298 K. (Isodesmic reactions are those in which the total number of each type

184

of bond is equal in reactants and products; the success of the method assumed to be associated with the cancellation of errors achieved through equating product and reactant bonds.) To implement the method, reactions involving the formation of molecules of interest and nH_2 (n=1, 2, or 3) from reactants with accepted $\Delta H_f(298)$ values were constructed. G03 calculations of reactant, product and reference molecule enthalpy differences at 298 K and 0 K $[H(298)-H(0)]$ were employed to derive $\Delta H_f(298)$ from QM results.

Condensed-phase densities $[\rho(298)]$ and heats of vaporization $[\Delta H_v(298)]$ were estimated via molecular dynamics (MD) simulations. Performed with the *Discover* program (Accelrys, Inc.) and employing the COMPASS force field[18], the simulations were performed with cubic, 3-D periodic cells of approximately 1250 atoms [56 to 72 molecules] constructed by the AmorphousCell module of InsightII. [Amorphous Cell builds cells according to a modified Markov process, incorporating rotational isomeric state probabilities modified to account for non-local (long-range) interactions[19,20].] Five different cells with an initial target density of 0.9 g/cc were built for each compound. The cube edge lengths produced by this procedure were approximately 25 Å. A group-based cut-off method with tail correction was employed to evaluate non-bond interactions. The cut-off method assumes that the radial distribution functions converge to unity beyond the cutoff distance. The cut-off distance was specified to be 10 Å for all compounds. The simulations consisted of three stages, the dynamics in all cases being modeled with Verlet velocity integration[21] and Andersen temperature control[22]. Berendsen pressure control[23] was employed for constant pressure simulations. The first stage was a 30,000 steps, 1-fs/step, constant volume and temperature (NVT) "pre-equilibration" simulation run to relieve large stresses (inadvertently) introduced by the cell packing procedure. The second stage of the procedure was a 30,000 steps, 1-fs/step constant pressure and temperature (NPT) simulation that allowed the cell to equilibrate. The final stage was a 50,000 step, 1-fs/step NPT simulation during which properties were recorded.

The study of the energetics of H-atom abstraction reactions is being conducted with the G03 implementation of CCSD/6-31+G(d,p), with some preliminary work being performed via MP2/6-31+G(d,p) calculations. Transition state searches were typically started via either QST2 or QST3 methods. The Gaussian-defined "tight" convergence criteria were employed to find a local minimum or transition state, and normal mode frequencies were calculated to confirm the nature of the structure.

Multiamines as Alternatives to MMH. Corroborating and extending research performed in the early to mid 1950's by the Phillips Petroleum Corporation, AMRDEC ignition delay test results were a basis for suggesting several multiamines to synthesize and evaluate, with two judged to hold considerable promise— 1,3-dimethylhexahydropyrimidine (DMHHP) and 1,3-dimethylimidizolidine (DMIZ). Variations on compounds with relatively short ignition delays, they were proposed as means of obtaining fuels with lower freezing points and higher specific impulses. However, these compounds are not commercially available, and there was a reluctance to undertake their synthesis without additional justification. The study summarized here was motivated by two papers discovered during a literature search for synthesis routes and properties of DMHHP. In the first, features of the gas-phase photoelectron spectra of DMHHP and some other cyclic multiamines were attributed to configuration-dependent lone pair "through-bond" and "through-space" interactions. The other paper reported that the H-2 NMR frequency (shifts) of 2-methyl- and 2-ethyl-1,3-diazanes were a strong function of substitute-dependent lone pair alignments. These observations suggested that ignition delay differences in a family of similar multiamines might be indicated on the basis of lone pair alignments.

To examine the possibility, the equilibrium geometries of 4 multiamines with measured ignition delays were determined. Two had relatively short ignition delays, one had a relatively long ignition delay, and one did not ignite. It was observed that in the compounds with long ignition delays, the lone pairs in the lowest energy, and therefore most highly populated; conformers aligned with at least one C-N bond while in the 2 compounds with short ignition delays, the sample would be dominated by conformers whose lone pairs did not align with a C-N bond. This correlation is shown graphically in Figure 10.

Given the correlation observed between a compound's ignition delay and the alignment of its lone-pairs with a C-N bond, the geometries DMHHP and DMIZ conformers were characterized. It was found that 298 K vapor samples of each compound would be dominated by conformers whose lone pairs do not align with a C-N bond. With this indication that the ignition delays of DMHHP and DMIZ would be short, their gas-phase enthalpies of formation were estimated via QM, their densities and enthalpies of vaporization were computed via molecular dynamics simulations, and these estimates were employed as input for thermochemical code predictions of their performance (in terms of density specific impulse) when oxidized by IRFNA. Shown in Table 1, the calculations indicate that DMHHP and DMIZ should yield performance that approaches that of MMH. Based on these findings, the synthesis and testing of DMHHP and DMIZ is to be pursued.

H-atom abstraction reaction energetics. The importance of H-atom abstraction reactions in the ignition of hydrazine-NO$_2$ systems was proposed by Sawyer and Glassman based on reaction rates, overall activation

energies and reaction orders observed for homogenous gas-phase reactions studied in an adiabatic flow reactor[24]. Similarly, the products observed from the gas-phase reaction of UDMH and NO_2 indicate that the first step is the abstraction of an H atom from a nitrogen site[25]. However, rate constants specific to the abstraction steps was not determinable from the experiments, and the systems are so large that they are only now computationally tractable at the level of theory needed to treat the electronic states involved.

At the time that this paper is being written, all of the stationary states for two H-atom abstraction reaction paths have been identified, one for hydrazine and on for MMH. Shown schematically in Figures 11 and 12, it is observed that the barrier to the abstraction of hydrogen from MMH is much lower than it is for hydrazine. Given that MMH has a shorter ignition delay than hydrazine, this result is consistent with the hypothesis that H-atom abstraction reactions are a rate limiting step. The estimation of a reaction rate constants based on the results remains to be performed.

4. Summary of Accomplishments and HPC Resources Utilized

(1) The application of modern computational fluid dynamics to the chemically reacting flow within the ISVE has yielded the first visualization of flow within the combustion chamber.
(2) It has been shown that the ARL multi-step reaction chemistry mechanism can be used to predict both the steady pressure level and the transient pressure peak caused by hypergolic initiation of propellants in the ISVE. The mechanism is computationally expensive but tractable on HPCs.
(3) The initial stages of validation of the ARL-NSRG3 CFD code have been completed; the code has been shown to be a useful design and evaluation tool for the ISVE.
(4) A correlation between a alkyl multiamine's ignition delay (when oxidized by IRFNA) and the orientation of it lone pair sites with respect to C-N or C-C bonds was observed and employed as a tool to predict (qualitatively) the ignition delay of notional hypergols.
(5) The energetics of abstractions of H-atoms from hydrazine and MMH by NO_2 have been determined and are consistent with their being a rate limiting step in the ignition process.

These accomplishments have been at the expense of about 13,000 hours on the ARSC Cray SV1, about 23,000 hours on the NAVO Cray SV1, about 18,000 hours on the ERDC SGI O3K, and about 120,000 hours on the ASC SGI O3K. The CFD code was run on the Cray's and the ERDC SGI while the CCM codes were executed in the ASC SGI. It is highly anticipated that the balance of 300,000 total HPC hours will be used in the next few months as further simulations are performed.

Table 1. Condensed-phase property and I_{sp} estimates for various diamines

Compound	p(298) (g/cc)		I_{sp}	$p^*I_{sp}(x10^{-3})$ (1b$_f$-s/ft^3)
	Lit.	Cal.		
Diamines				
TMEDA	0.78	0.78	280.6	13.7
DMIZ		0.83	279.8	14.5
DMPipZ	0.86	0.87	278.7	15.1
DMHHP		0.88	278.7	15.2
Hydrazines				
UDMH	0.79		285.9	14.0
Hydrazine	1.00		252.3	15.7
MMH	0.87		288.3	15.7

## Acknowledgements

References

1. Michaels, R.S. and B.F. Wilson, "The Low L/D Vortex Engine for Gel Propulsion." *Proceedings of the 1995 JANNAF Gel Propulsion Technology Symposium*, CPIA Pub. 627, Sept 1995, pp. 9–16.

2. Wilson, B.F. and J.W. Connaughton, "Investigation of a Unique Design Engine Assembly." *Proceedings of the 3rd AIAA Propulsion Joint Specialist Conference*, Washington, DC, 17–21 July 1967 (see also US Army MICOM Technical Report C67-7175, Redstone Army Arsenal, AL).

3. Nusca, M.J. and R.S. Michaels, "Development of a Computational Model for the Army's Impinging Stream Vortex Engine." *Proceedings of the 1st JANNAF Liquid Propellant Subcommittee Meeting*, Las Vegas, NV, May 2004, published by the CPIA.

4. Nusca, M.J., "Numerical Simulation of Electromagnetic Wave Attenuation in Nonequilibrium Chemically Reacting Flows." *Computers and Fluids*, Vol. 27, No. 2, 1998, pp. 217–238.

5. Nusca, M.J., "Numerical Simulation of the Ram Accelerator Using a New Chemical Kinetics Mechanism." *Journal of Propulsion and Power*, Vol. 18, No. 1, January–February 2002, pp. 44–52.

6. Chew, W.M., D.L. May, and D.M. Thompson, "Non-Newtonian Rheology of Gelled Propellants." *Proceedings of the 1998 JANNAF Propulsion Meeting*, CPIA Pub. 675, Vol. 1, July 1998, pp. 141–149.

7. Rahimi, S. and B. Natan, Numerical Solution of the Flow of Power-Law Gel Propellants in Converging Injectors." *Propellants, Explosives. Pyrotechnics*, Vol. 25, No. 1, 2000, pp. 203–212 (also, *Journal of Propulsion and Power*, Vol. 16, No. 3, May–June 2000, pp. 458–464.

8. Spalart, P.R. and S.R. Allmaras, "A One-Equation Turbulence Model for Aerodynamic Flows." *AIAA Paper No. 92-0439*, Jan 1992.

9. McBride, B.J. and S. Gordon, "Computer Program for Calculation of Complex Chemical Equilibrium Compositions and Applications, II. Users Manual and Program Description." *NASA RP 1311*, 1996.

10. Miller, R.S, K. Harstad, and J. Bellan, "Evaluation of Equilibrium and Non-Equilibrium Evaporation Models for Many-Droplet Gas-Liquid Flow Simulations." *International J. of Multiphase Flow*, 24, N6, 1998, pp. 1025–1055.

11. Frisch, M.J., and G.W.Trucks, et al., Gaussian 03, Revision B.05, Gaussian, Inc., Pittsburgh, PA, 2003.

12. Perdew, J.P, K. Burke, and M. Ernzerhof, "Generalized gradient approximation made simple." *Physical Review Letters*, vol. 77, 1996, pp. 3865–3868.

13. Perdew, J.P., K. Burke, and M. Ernzerhof, "Generalized gradient approximation made simple." *Physical Review Letters*, vol. 78, 199, p. 13967.

14. Miehlich, B., A. Savin, H Stoll, and H. Preuss, "Results Obtained with the Correlation-Energy Density Functionals of Becke and Lee, Yang and Parr." *Chemical Physics Letters*, vol. 157, 1989, pp. 200–206.

15. Clark, T., J. Chandrashakar, G.W. Spitznagel, , and P.V.R. Schleyer, "Efficient Diffuse Function-Augmented Basis-Sets for Anion Calculations. 3. The 3-21+G Basis Set for 1st-Row Elements, Li-F." *Journal of Computational Chemistry*, vol. 4, 1983, pp. 294–301.

16. McLean, A.D. and G.S. Chandler, "Contracted Gaussian-Basis Sets For Molecular Calculations. 1. 2nd Row Atoms, Z=11–18." *Journal of Chemical Physics*, vol. 72, 1980, pp. 5639–5648.

17. Krishnan, R., J.S. Binkley, R. Seeger, and J.A. Pople, "Self-Consistent Molecular-Orbital Methods. 20. Basis Set for Correlated Wave-Functions." *Journal of Chemical Physics*, vol. 72, 1980, pp. 650–654.

18. Sun, H., "COMPASS: An *ab initio* force-field optimized for condensed-phase applications - Overview with details on alkane and benzene compounds." *Journal of Physical Chemistry B.*, vol. 102, 1998, pp. 7338–7364.

19. Theodorou, D.N. and U.W. Suter, "Atomistic Modeling of Mechanical-Properties of Polymeric Glasses." *Macromolecules*, vol. 19, 1986, pp. 139–154.

20. Meirovitch, H., "Computer-Simulation of Self-Avoiding Walks - Testing the Scanning Method." *Journal of Physical Chemistry*, vol. 79, 1983, pp. 502–508.

21. Swope W.C., H.C. Andersen, P.H. Berens, and K.R. Wilson, "A Computer-Simulation Method for the Calculation of Equilibrium-Constants for the Formation of Physical Clusters of Molecules - Application to Small Water Clusters." *Journal of Physical Chemistry*, vol. 76, 1982, pp. 637–649.

22. Andrea, T.A., W.C. Swope, and H.C. Andersen, "The Role of Long Ranged Forces in Determining the Structure and Properties of Liquid Water." *Journal of Chemical Physics*, vol. 79, 1983, pp. 4576–4584.

23. Berendsen, H.J.C., J.P.M. Postma, W.F. van Gunsteren, A. DiNola, and J.R. Haak, "Molecular-Dynamics with Coupling to an External Bath." *Journal of Chemical Physics*, vol. 81, 1984, pp. 3684–3690.

24. Sawyer, R.F. and I. Glassman, "Gas-Phase Reactions of Hydrazine with Nitrogen Dioxide, Nitrogen Oxide, and Oxygen." *Proceeding of the 11th Symposium (International) on Combustion*, 1967, pp. 861–869.

25. Tuazon, E.C., W.P.L. Carter, R.V. Brown, A.M. Winer, and J.N. Pitts, "Gas-Phase Reaction of 1,1-Dimethylhydrazine with Nitrogen Dioxide." *Journal of Physical Chemistry*, vol. 87, 1983, pp. 1600–1605.
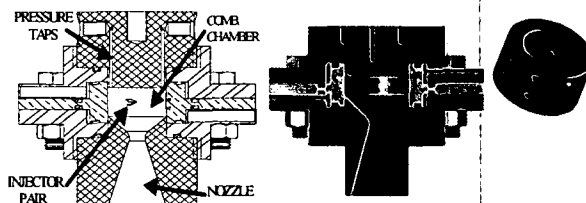
Figure 1. Schematics of the ISVE in an engine test block
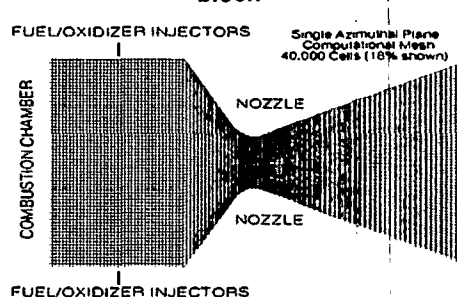
Figure 2. Computational grid for ISVE showing a single azimuthal plane containing two pairs of opposed injectors (not all cells plotted for clarity)
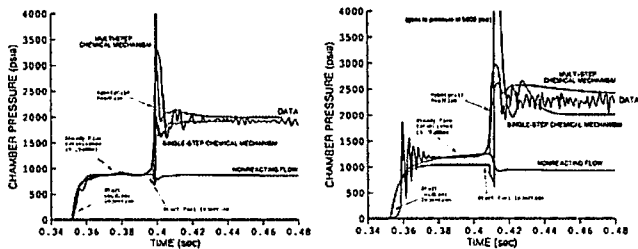
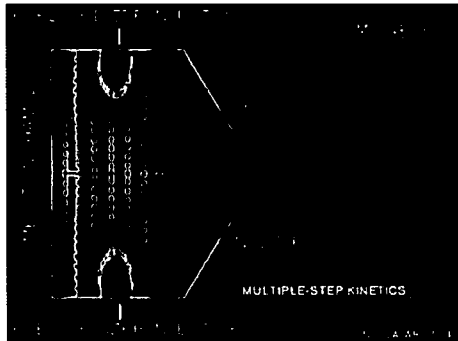Figure 3. Measured and computed chamber pressures: Engine No. 1 (left) and Engine No. 5 (right)

Figure 4. Computed pressure contours (blue to red: 0 to 2 kpsia) and selected velocity vectors at .43 seconds for Engine No. 1

Figure 5. Computed pressure contours (blue to red: 0 to 3 kpsia) and selected velocity vectors at .45 seconds for Engine No. 5
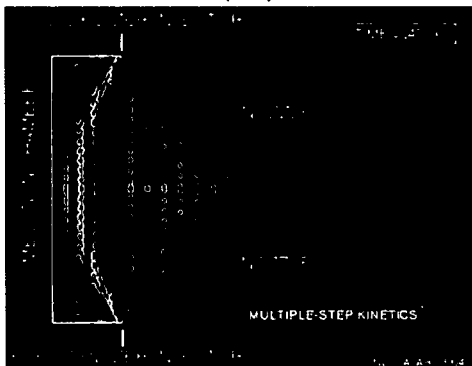
Figure 6. Computed product (OH) mass fraction contours (blue to red: 0 to .8) and selected velocity vectors at .43 seconds for Engine No. 1
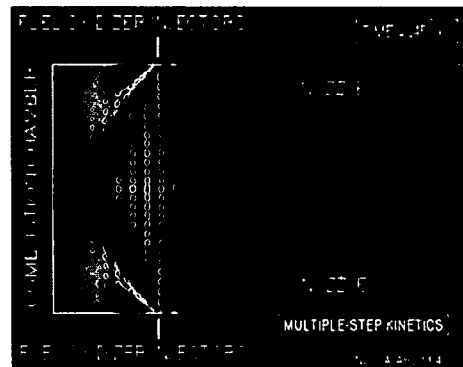
Figure 7. Computed product (OH) mass fraction contours (blue to red: 0 to .8) and selected velocity vectors at .45 seconds for Engine No. 5
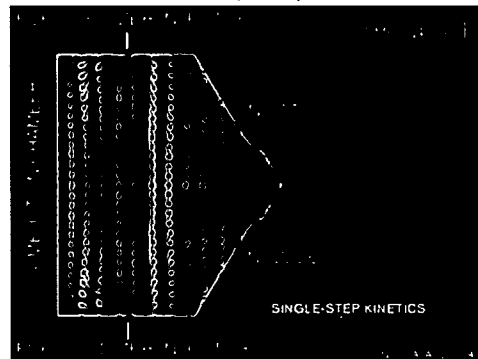
Figure 8. Computed product (OH) mass fraction contours (blue to red: 0 to .012) and selected velocity vectors at .43 seconds for Engine No. 1

Figure 9. Computed product (OH) mass fraction contours (blue to red: 0 to .012) and selected velocity vectors at .45 seconds for Engine No. 5
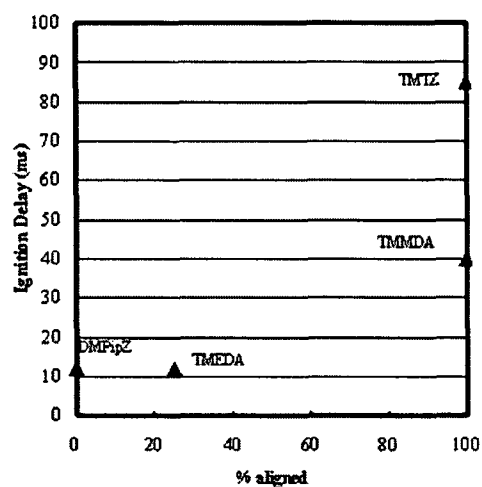
Figure 10. Comparison of the total statistical weight of a compound's conformers with "aligned" lone pairs (at 298 K) and their ignition delay
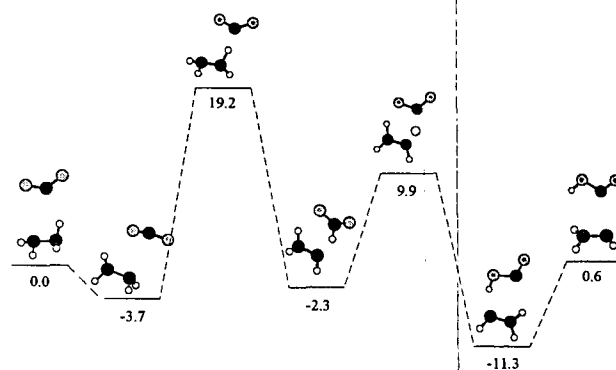

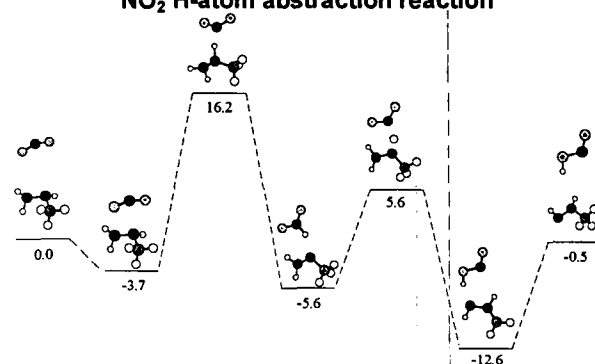Figure 11. The energetics (kcal/mol) of a hydrazine + NO_2 H-atom abstraction reaction

Figure 12. The energetics (kcal/mol) of a MMH + NO_2 H-atom abstraction reaction